Title: Structural and Spectroscopic Characterization of a High-Spin FeNO6 Complex with an Iron(IV)-NO- Electronic Structure

Authors: Amy Speelman; Bo Zhang; Carsten Krebs; Nicolai Lehnert

To be cited as: 10.1002/anie.201601742

Link to VoR: http://dx.doi.org/10.1002/anie.201601742

Structural and Spectroscopic Characterization of a High-Spin {FeNO}^{6} Complex with an Iron(IV)-NO Electronic Structure

Amy L. Speelman, Bo Zhang, Carsten Krebs, and Nicolai Lehnert*

Abstract: Although the interaction of low-spin ferric complexes with nitric oxide has been well studied, examples of stable high-spin ferric nitrosyls (such as those that could be expected to form at typical non-heme iron sites in biology) are extremely rare. Using the TMG_3tren co-ligand, we have prepared a high-spin ferric NO adduct ({FeNO}^{6} complex) via electrochemical or chemical oxidation of the corresponding high-spin ferrous NO {FeNO}^{7} complex. The {FeNO}^{6} compound is characterized by UV-Visible and IR spectroelectrochemistry, Mössbauer spectroscopy, NMR, x-ray crystallography, and DFT calculations. The data show that its electronic structure is best described as a high-spin iron(IV) center bound to a triplet NO ligand with a very covalent iron-NO bond. This finding demonstrates that high-spin iron nitrosyl compounds undergo ***iron-centered*** redox chemistry, leading to fundamentally different properties than corresponding low-spin compounds, which undergo ***NO-centered*** redox transformations.

Nitric oxide (NO) is known to have a variety of effects in mammalian systems, ranging from nanomolar concentration, where it acts as a signaling molecule, to micromolar concentration, where it acts as an immune defense agent.[1] Many of the effects of nitric oxide are mediated by interaction with metal centers, particularly iron. Although the interaction of NO with both ferric and ferrous heme iron has been well-studied[2], the interaction of NO with high-spin non-heme iron centers, particularly in the ferric case, is not as well understood. Correspondingly, although multiple low-spin (diamagnetic) ferric NO adducts ({FeNO}^{6} in the Enemark-Feltham notation[3]) are known in the literature, only one well-characterized high-spin (paramagnetic) {FeNO}^{6} complex has been reported to date.[4-5] However, this complex employs a tri-anionic tripodal thiolate ligand and is therefore dissimilar to typical biological non-heme iron sites. On the other hand, as has been shown previously, the neutral TMG_3tren ligand (Scheme 1) is able to stabilize iron in high oxidation states due to its strong donicity and typically favors high-spin electronic configurations.[7] This precedent suggests that it may be possible to generate a rare high-spin {FeNO}^{6} species (**1**) from the corresponding {FeNO}^{7} complex

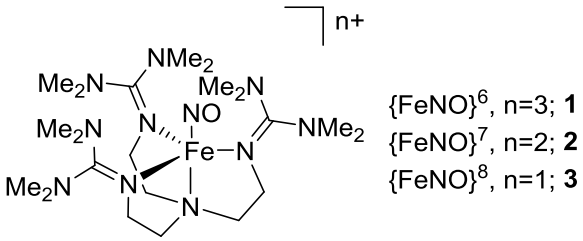

(**2**) previously reported by our group.[8]

Scheme 1. Structure of the TMG_3tren iron nitrosyl complex.

Here, we report the synthesis of a high-spin {FeNO}^{6} complex $[Fe(TMG_3tren)(NO)]^{3+}$ (**1**) generated via oxidation of **2**, which is the first example of a paramagnetic {FeNO}^{6} compound with a neutral co-ligand. This is also the first paramagnetic {FeNO}^{6} complex that can be characterized in the corresponding {FeNO}^{7} and {FeNO}^{8} oxidation states. The spectroscopic parameters and structural features of **1** are used to demonstrate that this complex is best described as a high-spin Fe(IV)-NO species. Finally, the electronic structures of the set of TMG_3tren {FeNO}$^{6-8}$ complexes are contrasted to those of corresponding low-spin systems.

Previously, we reported that **2** undergoes a reversible one-electron reduction at -1.34 V vs ferrocene to yield a metastable {FeNO}^{8} complex (**3**).[8] The cyclic voltammogram of **2** in acetonitrile also exhibits a chemically reversible {FeNO}$^{6/7}$ couple at +0.67 V vs ferrocene (Figure S1). In order to determine the spectroscopic features of the oxidized compound (**1**), we first performed UV-Visible (Figure 1) and infrared (Figure 2) spectroelectrochemistry experiments.

In the UV-Vis spectrum, the high-intensity band at 365 nm (= 6,300 $M^{-1}cm^{-1}$) in **2** is replaced by two features at 394 nm (= 5,400 $M^{-1}cm^{-1}$) and 515 nm (= 6,100 $M^{-1}cm^{-1}$) upon oxidation, corresponding to a color change from pale brown to deep red. A similar change in the absorption spectrum was reported for the oxidation of a TMG_3tren Fe(III)-CN complex to an Fe(IV)-CN complex; in this case, the high-intensity bands were assigned as LMCT bands originating from the TMG_3tren ligand.[7c] The analogous changes in UV-Vis features upon oxidation of **2** to **1** hint at an unusual Fe(IV) oxidation state for **1** (since **2** is best described as an Fe(III)-NO complex). Additionally, upon oxidation of **2** to **1** an extremely broad, low-intensity band grows in at ~980 nm (≈ 440 $M^{-1}cm^{-1}$). A similar feature has been observed in the TMG_3tren Fe(IV)=O complex, and was assigned as an (d_{xz}/d_{yz} d_{z2}) transition[7d], which further suggests that **1** could have a similar high-spin d^4 electron configuration.

[*] A.L. Speelman, Prof. N. Lehnert
Department of Chemistry
University of Michigan
930 N University Avenue
Ann Arbor, MI 48109 (USA)
E-mail: lehnertn@umich.edu

Dr. B. Zhang, Prof. C. Krebs
Department of Chemistry
Department of Biochemistry and Molecular Biology
The Pennsylvania State University
University Park, PA 16802 (USA)

Supporting information for this article is given via a link at the end of the document.

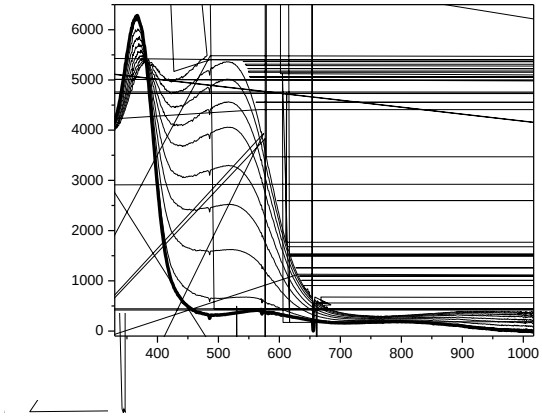

Figure 1. UV-Visible spectroelectrochemistry showing the oxidation of **2** to **1** in CH_3CN.

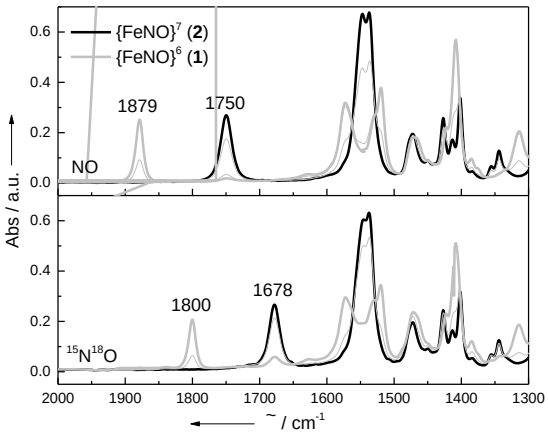

Figure 2. IR spectroelectrochemistry showing the oxidation of **2** to **1** (top) and **2**-$^{15}N^{18}O$ to **1**-$^{15}N^{18}O$ (bottom) in CD_3CN.

In the IR spectrum, the N-O stretch of **2** at 1750 cm^{-1} is replaced by a peak at 1879 cm^{-1} upon oxidation, which can be assigned as the N-O stretch based on comparison to the $^{15}N^{18}O$ isotopolog. The magnitude of the upshift upon oxidation is relatively small and is nearly identical to the 130 cm^{-1} *downshift* observed in the iron-centered reduction of **2** to **3**[8], implying that the oxidation of **2** to **1** is also iron-centered.

Complex **1** can be generated in bulk by chemical oxidation with the radical cation of thianthrene (see Figures S2-S4). The ^1H NMR spectrum of **1** exhibits broad, paramagnetically shifted resonances (Figure S5) and a solution magnetic moment of 3.2 $_B$ (determined using the Evans method) indicative of an S = 1 spin state, which is consistent with the other reported paramagnetic $\{FeNO\}^6$ complexes.[4]

In order to further characterize the series of $\{FeNO\}^{6-8}$ complexes, Mössbauer spectra of frozen solutions of **1**-**3** were recorded (Table 1, Figures S6-S8). Due to the generally observed non-innocence of NO as a ligand, the redox state of the iron center cannot be definitively assigned by the isomer shift ( ) alone, since is correlated with both Fe-ligand -bonding and iron oxidation state.[9] However, the relatively large magnitude of the stepwise change in along the $\{FeNO\}^{6-8}$ series is suggestive of iron-centered redox chemistry (Table 1). Interestingly, both and the quadrupole splitting ($|\Delta E_Q|$) of **1** are extremely similar to the values for the S = 2 TMG_3tren Fe(IV)=O complex[7a]. This is due to the fact that NO , like the oxo ligand, acts primarily as a -donor in high-spin complexes (see below). This observation implies an Fe(IV)-NO electronic structure for **1**. In contrast, the Mössbauer parameters of the S = 0 Fe(IV)-CN complex[7c] are significantly different from those of **1**.

Although unstable at room temperature, **1** is sufficiently stable at -35°C to allow for crystallization (Figure 3, Table 1).[10] The Fe-N-O bond of **1** is completely linear, compared to the bent Fe-N-O bond of **2**[8] and other $\{FeNO\}^7$ complexes.[11] Linearization of the Fe-NO bond in $\{FeNO\}^6$ complexes has been observed previously for low-spin systems.[2] Oxidation leads to a decrease in the Fe-N(O) bond length in **1** as compared to **2**, whereas the N-O bond length is only marginally decreased in **1**. Although no structural characterization is available for the $\{FeNO\}^7$ form of [Fe(PS3*)(NO)] (which is the only other structurally characterized paramagnetic $\{FeNO\}^6$ complex), the $\{FeNO\}^7$ form of the closely related complex [Fe(NS3)(NO)] was structurally characterized; the geometric differences between the $\{FeNO\}^6$ and $\{FeNO\}^7$ compounds are qualitatively similar to those in **1** and **2** (Table 1).[4] Interestingly, the bonds to the TMG_3tren co-ligand in **1** are much shorter than those reported for any other iron-TMG_3tren structure, including the analogous Fe(IV)=O complex (Table 1) which again strongly implies an Fe(IV) center for **1**.[7b] Taken together, the structural and spectroscopic data all support the assignment of **1** as an Fe(IV)-NO species.

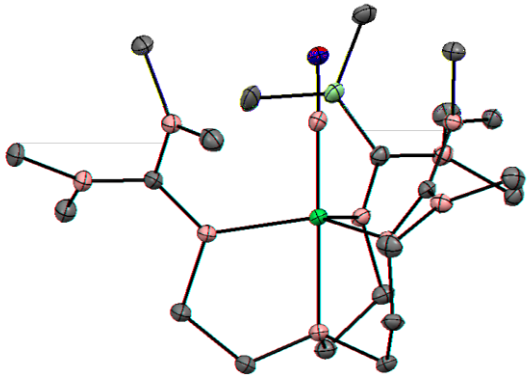

Figure 3. Crystal structure of **1** with thermal ellipsoids shown at 30% probability. Hydrogen atoms, solvent (CH_3CN) molecules, and tetrafluoroborate counterions have been omitted for clarity.

To gain further insight into the nature of the bonding in this system, density functional theory (DFT) calculations were employed. The calculated geometric and spectroscopic parameters of **1**, **2**, and **3** are all in excellent agreement with experimental values (Tables S2-S3). In particular, the DFT-calculated and experimental show a strong linear correlation (Figure 4), which indicates that DFT is able to properly describe

Table 1. Comparison of structural and spectroscopic parameters for the TMG_3tren $\{FeNO\}^{6-8}$ series to selected compounds from the literature.

	Fe-N (Å)	N-O (Å)	Fe-N-O (°)	Avg. Fe-N_{guan} (Å)	Fe-$_{amine}$ (Å)	*S*	(mm/s)	$\|\Delta E_Q\|$ (mm/s)	(NO) (cm^{-1})	Ref.
$\{FeNO\}^6$, **1**	1.680	1.142	179.9	1.966	2.020	1	0.06[a]	0.48[a]	1879[b]	*t.w.*
$\{FeNO\}^7$, **2**	1.748	1.154	168.0	2.037	2.251	3/2	0.48[a]	1.42[a]	1750[b]	[8], *t.w.*
$\{FeNO\}^8$, **3**						1	0.84[a]	2.78[a]	1618[b]	[8], *t.w.*
$[Fe^{IV}(TMG_3tren)(O)]^{2+}$				2.006	2.112	2	0.09[c]	0.29[c]		[7a, 7b]
$[Fe^{IV}(TMG_3tren)(CN)]^{3+}$						0	-0.19[c]	4.45[c]		[7c]
$\{FeNO\}^6$ [Fe(PS3*)(NO)]	1.676	1.154	175.2			1			1807[d]	[4]
$\{FeNO\}^7$ [Fe(NS3)(NO)]	1.756	1.11 1.18	145.9 147.8		2.178	3/2			1639[d]	[4]

[a] Measured at 4.2 K in frozen 1:1 propionitrile:butyronitrile solution [b] In CH_3CN solution [c] Measured at 4.2 K in frozen CH_3CN solution [d] Nujol mull

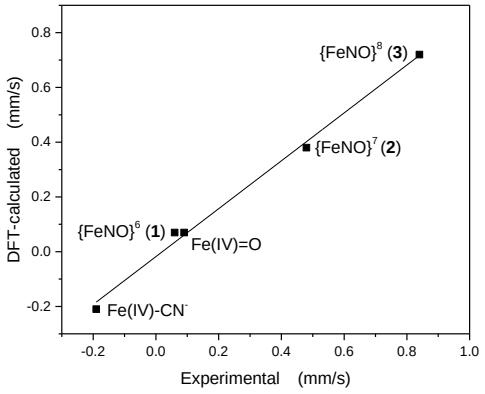

Figure 4. Correlation of experimental and DFT-calculated (at the B3LYP level) for **1**-**3** and selected TMG_3tren compounds (see Table 1).

bonding trends within this series. As reported previously, the electronic structure of **2**[8] and other high-spin $\{FeNO\}^7$ complexes[11-12] is best described as a high-spin Fe(III) center antiferromagnetically coupled to triplet NO . The NO in these systems acts as a weak -acceptor (α-spin), but mainly as a strong -donor (β-spin) into the iron d_{xz} and d_{yz} orbitals (where the z-axis lies along the Fe-N(O) bond vector), resulting in a highly covalent Fe-NO bond.[13] The DFT calculations reveal an Fe(IV)-NO electronic structure for **1** consistent with experimental findings. Due to the higher effective nuclear charge of the iron center in **1** as compared to **2**, the NO moiety donates additional electron density into the Fe d-orbitals in **1**, making the Fe-NO bond even more covalent. This finding is consistent with a previous study which showed that Fe-NO bond covalency increases with increasing effective nuclear charge of the iron center in a series of $\{FeNO\}^7$ complexes.[13] The increase in the covalency of the Fe-NO bond is reflected by the composition of the magnetic orbitals (Figure 5, bottom), where the orbitals of **1** show increased Fe character as compared to **2**. On the other hand, upon reduction of **2** to the $\{FeNO\}^8$ (Fe(II)-NO) complex **3**, a decrease in the covalency of the Fe-NO bond is observed.

In contrast to the iron-centered redox chemistry for the high-spin complexes **1**-**3**, the redox chemistry in low-spin iron nitrosyl systems has been shown to be NO-centered, which is supported by the spectroscopic features of these complexes. For example, in the $[Fe(cyclam\text{-}ac)(NO)]^n$ (n = 0, +1, +2) system, N-O stretching frequencies of 1903 cm^{-1}, 1607 cm^{-1}, and 1271 cm^{-1} and of 0.01 mm/s, 0.26 mm/s, and 0.41 mm/s are observed for the $\{FeNO\}^6$, $\{FeNO\}^7$, and $\{FeNO\}^8$ complexes, respectively. The large changes in N-O stretching frequencies and small changes in are in accordance with more NO-centered redox chemistry in low-spin systems.[14] Heme complexes generally behave in a similar way. Thus, in heme systems, the N-O stretching frequencies for 5-coordinate $\{FeNO\}^6$, $\{FeNO\}^7$, and $\{FeNO\}^8$ complexes are approximately 1850 cm^{-1}, 1680 cm^{-1}, and 1460 cm^{-1}, respectively.[2, 15]

In the TMG_3tren system, however, the N-O stretch increases only moderately (approximately 130 cm^{-1}) upon oxidation, and the Mössbauer isomer shift decreases more dramatically (approximately 0.4 mm/s) in line with the fact that the redox chemistry is iron-centered. These results show how the electronic structures of iron nitrosyls are dependent on the spin state. We are currently investigating the reactivity differences that result from this. In particular, low-spin heme $\{FeNO\}^6$ complexes are known to be electrophilic due to their $Fe(II)\text{-}NO^+$ electronic structure.[2] In contrast, since **1** has an Fe(IV)-NO electronic structure and a highly covalent Fe-NO bond, the complex is not expected to be appreciably electrophilic. Additionally, low-spin ferric nitrosyl model complexes are intrinsically unstable with respect to NO loss[2], whereas NO loss from **1** is not observed even under vacuum (Figure S9).

In summary, complexes **1**-**3** represent the first reported high-spin $\{FeNO\}^{6-8}$ series. Our data show that the $\{FeNO\}^6$, $\{FeNO\}^7$, and $\{FeNO\}^8$ complexes have Fe(IV)-NO , Fe(III)-NO , and Fe(II)-NO electronic structures, respectively, indicating that in high-spin non-heme iron nitrosyl complexes, all redox chemistry is iron-centered. Our current efforts are focused on .performing detailed spectroscopic analyses of these complexes as well as a corresponding $\{FeHNO\}^8$ complex, including MCD high-field Mössbauer, NRVS, and EXAFS, in order to further validate the proposed electronic structures of these systems.

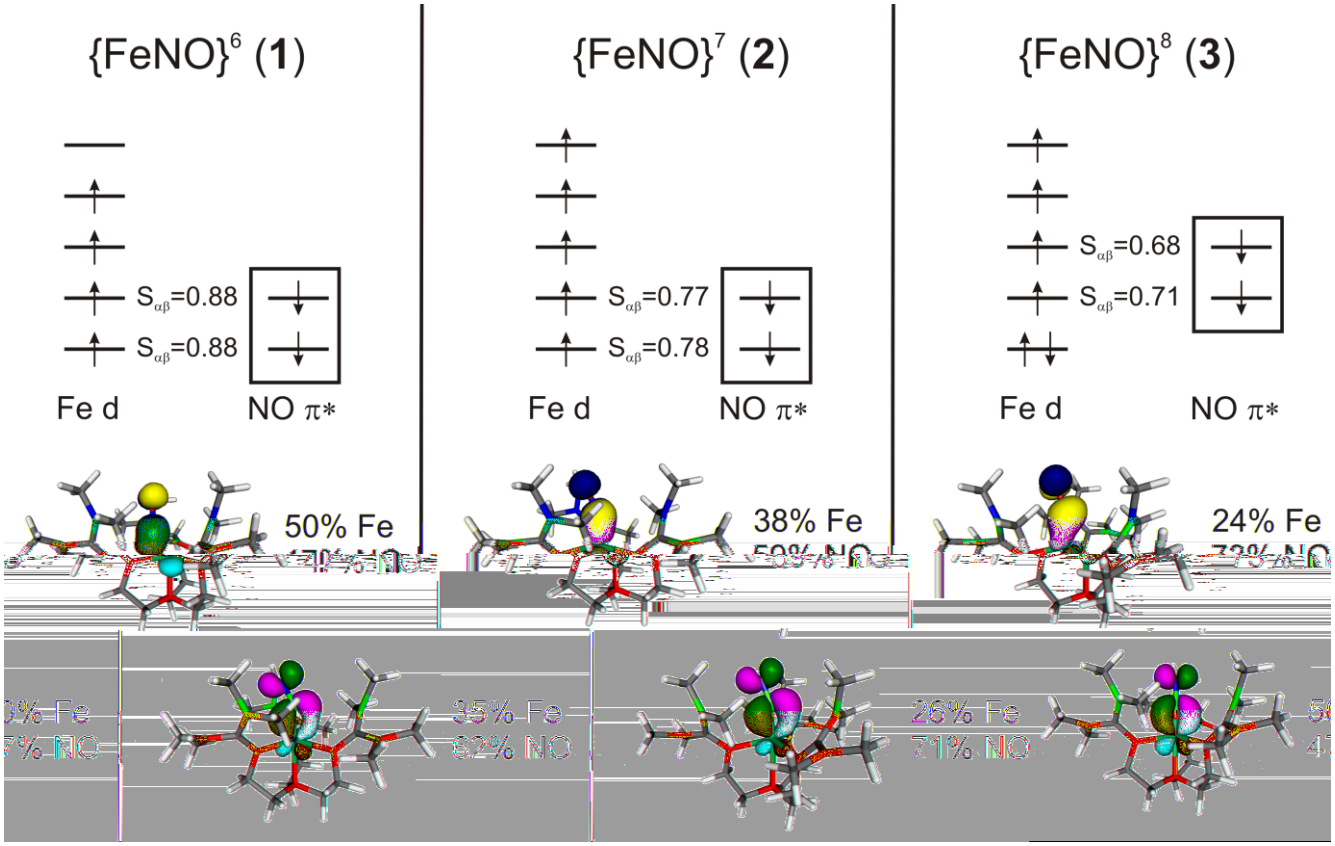

Figure 5. Schematic MO diagrams for the high-spin TMG_3tren $\{FeNO\}^{6-8}$ series. The -spin magnetic orbitals (boxed), which constitute the primary Fe-NO bonding interaction (NO to Fe donation), are shown with the percentage of iron and NO character indicated. S_α denotes the overlap between the α-spin and -spin orbitals and is an indicator of covalency in the Fe-NO unit (a larger S_α indicates a more covalent bond).

Acknowledgements

This research was supported by the National Science Foundation (CHE-1305777 to N.L.) A.L.S. acknowledges support from an NSF Graduate Research Fellowship (DGE-0718128) and a Rackham Predoctoral Fellowship (University of Michigan). We acknowledge Dr. Jeff Kampf (University of Michigan) for the X-ray crystallographic analysis of **1** and the NSF for instrumentation (CHE-0840456).

Keywords: Bioinorganic chemistry • Enzyme Models • Nitric oxide • Nitrogen oxides • Non-heme iron

[1] *Nitric Oxide: Biology and Pathobiology*, (Ed: L. J. Ignarro) Academic Press, San Diego, **2010**.

[2] N. Lehnert, W. R. Scheidt, M. Wolf, *Struct. Bond.* **2014**, *154*, 155-223.

[3] In the Enemark-Feltham notation, metal nitrosyls are denoted by $\{MNO\}^X$ where X is the number of iron d plus NO * electrons.[4]

[4] J. Conradie, D. A. Quarless, H.-F. Hsu, T. C. Harrop, S. J. Lippard, S. A. Koch, A. Ghosh, *J. Am. Chem. Soc.* **2007**, *129*, 10446-10456.

[5] Two other $\{FeNO\}^6$ complexes have been suggested to be paramagnetic (S = 1), but in these cases the proposed spin state was not proven experimentally.[6]

[6] a) M. J. Rose, N. M. Betterley, A. G. Oliver, P. K. Mascharak, *Inorg. Chem.* **2010**, *49*, 1854-1864; b) M. D. Pluth, S. J. Lippard, *Chem. Commun.* **2012**, *48*, 11981-11983.

[7] a) J. England, M. Martinho, E. R. Farquhar, J. R. Frisch, E. L. Bominaar, E. Münck, L. Que Jr., *Angew. Chem.* **2009**, *121*, 3676-3680; *Angew. Chem. Int. Ed.* **2009**, *48*, 3622-3626; b) J. England, Y. Guo, E. R. Farquhar, V. G. Young Jr, E. Münck, L. Que Jr., *J. Am. Chem. Soc.* **2010**, *132*, 8635-8644; c) J. England, E. R. Farquhar, Y. Guo, M. A. Cranswick, K. Ray, E. Münck, L. Que Jr., *Inorg. Chem.* **2011**, *50*, 2885-2896; d) M. Srnec, S. D. Wong, J. England, L. Que Jr., E. I. Solomon, *Proc. Natl. Acad. Sci. USA* **2012**, *109*, 14326-14331.

[8] A. L. Speelman, N. Lehnert, *Angew. Chem.* **2013**, *125*, 12509-12513; *Angew. Chem. Int. Ed.* **2013**, *52*, 12283-12287.

[9] M. Li, D. Bonnet, E. Bill, F. Neese, T. Weyhermüller, N. Blum, D. Sellmann, K. Wieghardt, *Inorg. Chem.* **2002**, *41*, 3444-3456.

[10] Experimental details for the acquisition of crystal data and structure refinement can be found in the Supporting Information. CCDC 1450725 contains the supplementary crystallographic data for this paper. These data can be obtained free of charge from the Cambridge Crystallographic Data Centre via www.ccdc.cam.ac.uk/data_request/cif

[11] T. C. Berto, A. L. Speelman, S. Zheng, N. Lehnert, *Coord. Chem. Rev.* **2013**, *257*, 244-259.

[12] C. A. Brown, M. A. Pavlosky, T. E. Westre, Y. Zhang, B. Hedman, K. O. Hodgson, E. I. Solomon, *J. Am. Chem. Soc.* **1995**, *117*, 715-732.

[13] T. C. Berto, M. B. Hoffman, Y. Murata, K. B. Landenberger, E. E. Alp, J. Zhao, N. Lehnert, *J. Am. Chem. Soc.* **2011**, *133*, 16714-16717.

[14] R. Garcia-Serres, C. A. Grapperhaus, E. Bothe, E. Bill, T. Weyhermüller, F. Neese, K. Wieghardt, *J. Am. Chem. Soc.* **2004**, *126*, 5138-5153.

[15] L. E. Goodrich, S. Roy, E. E. Alp, J. Zhao, M. Y. Hu, N. Lehnert, *Inorg. Chem.* **2013**, *52*, 7766-7780.

Entry for the Table of Contents (Please choose one layout)

Layout 2:

COMMUNICATION

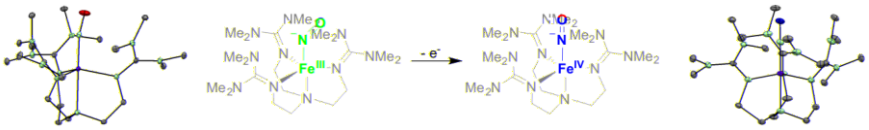

One-electron oxidation of the high-spin ferrous nitrosyl complex $[Fe(TMG_3tren)(NO)]^{2+}$ yields a rare high-spin (S = 1) ferric NO adduct ($\{FeNO\}^6$). Spectroscopic investigations and DFT calculations indicate that this species has an Fe(IV)-NO electronic structure. This finding demonstrates that high-spin non-heme iron nitrosyl complexes have fundamentally different redox behavior compared to corresponding low-spin heme systems.

*Amy L. Speelman, Bo Zhang, Carsten Krebs, and Nicolai Lehnert**

Page No. – Page No.

Structural and Spectroscopic Characterization of a High-Spin $\{FeNO\}^6$ Complex with an Iron(IV)-NO Electronic Structure

Table of Contents

Synthetic Procedures

Preparation and handling of air sensitive materials was carried out under a dinitrogen atmosphere in an MBraun glovebox equipped with a circulating purifier (O_2, $H_2O < 0.1$ ppm) or by using standard Schlenk techniques. Solvents and reagents were purchased and used as supplied except as follows. Acetonitrile, deuterated acetonitrile, propionitrile, and butyronitrile were distilled from calcium hydride, and diethyl ether was distilled from sodium benzophenone. All solvents were freeze-pump-thawed to remove dioxygen and stored over molecular sieves. Nitric oxide (Cryogenic Gases Inc., 99.5%) was purified by passage through an ascarite II column (NaOH on silica) followed by a cold trap at -80°C in order to remove higher nitrogen oxide impurities. Nitric oxide-$^{15}N^{18}O$ (Sigma-Aldrich) was used without further purification. Tetrabutylammonium hexafluorophosphate was recrystallized from ethanol. Thianthrene tetrafluoroborate was prepared by oxidation of thianthrene with nitrosonium tetrafluoroborate following a literature procedure.[1] $[Fe(TMG_3tren)(NO)](OTf)_2$ was prepared as previously described.[2] $Fe(CH_3CN)_6(BF_4)_2$ was synthesized by oxidation of iron powder with nitrosonium tetrafluoroborate following a literature procedure.[3] $[Fe(TMG_3tren)(NO)](BF_4)_2$ was synthesized by metalation of the TMG_3tren ligand with $Fe(CH_3CN)_6(BF4)_2$ followed by exposure to excess NO gas in a manner analogous to the triflate complex.[2] ^{57}Fe complexes (with tetrafluoroborate counterions) were synthesized in a manner analogous to the natural abundance complexes. The solution of the $\{^{57}FeNO\}^8$ complex used for Mössbauer spectroscopy was generated by reduction of the corresponding $\{^{57}FeNO\}^7$ complex with 1.2 equivalents of bis(pentamethylcyclopentadienyl)cobalt(II) as previously described.[2]

The $\{FeNO\}^6$ complex $[Fe(TMG_3tren)(NO)]^{3+}$ (**1**) was prepared by addition of a slight excess (1.2-1.5 equivalents) of thianthrene tetrafluoroborate to $[Fe(TMG_3tren)(NO)](X)_2$ (**2**; X = OTf or BF_4), typically in the 5-15 mM concentration range with respect to Fe, in CH_3CN. The $\{FeNO\}^6$ complex can be precipitated by addition of diethyl ether to these solutions (Fig. S4), but since precipitation generally leads to partial decomposition, all characterization was carried out on freshly prepared solutions of the complex. EPR (Figure S3), solution IR (Figure S2), and/or NMR (Figure S5) spectroscopy were used to confirm sample purity. The $\{^{57}FeNO\}^6$ solution used for Mössbauer spectroscopy was prepared in a manner analogous to the unlabeled compound.

Physical measurements

Infrared spectra of solid samples were obtained from KBr disks on Perkin-Elmer BX, GX, or RX1 spectrometers, and the IR spectra of solution samples were obtained in cells equipped with CaF_2 windows on the same instruments. Proton NMR spectra were recorded on a Varian MR 400 MHz instrument or a Varian VNMRS 500 MHz instrument. Solution magnetic susceptibility measurements were performed on

[1] B. Boduszek, H. J. Shine, *J. Org. Chem.* **1988**, *53*, 5142-5143.
[2] A. L. Speelman, N. Lehnert, *Angew. Chem.* **2013**, *125*, 12509-12513; *Angew. Chem. Int. Ed.* **2013**, *52*, 12283-12287.
[3] a) R. A. Heintz, J. A. Smith, P. S. Szalay, A. Weisgerber, K. R. Dunbar, in *Inorganic Syntheses, Vol. 33* (Ed.: D. Coucouvanis), John Wiley & Sons, Inc., **2002**, pp. 75-121. b) B. J. Hathaway, D. G. Holah, A. E. Underhill, *J. Chem. Soc.* **1962**, 2444-2448. c) B. J. Hathaway, A. E. Underhill, *J. Chem. Soc.* **1960**, 3705-3711.

a Varian MR 400 MHz instrument at 295 K using the Evans method.[4] Diamagnetic corrections were determined from Pascal's constants. Electronic absorption spectra were recorded using an Analytical Jena Specord S600 instrument. Electron paramagnetic resonance spectra were measured on a Bruker X-Band EMX spectrometer equipped with an Oxford Instruments liquid helium cryostat. Cyclic voltammograms were obtained using a CH instruments CHI600E electrochemical workstation using a three component system consisting of a glassy carbon working electrode, a platinum counter electrode, and a silver wire pseudo-reference electrode. Potentials were corrected to Fc/Fc^{+} using an internal ferrocene standard. UV-Visible and IR spectroelectrochemistry experiments were performed using custom-built thin layer electrochemical cells as previously described.[5] All electrochemical and spectroelectrochemical measurements were performed in the presence of 0.1 M tetrabutylammonium hexafluorophosphate as supporting electrolyte.

Mössbauer spectra were recorded on spectrometers from SEECO (Edina, MN). The spectrometer used to record the weak-field spectra is equipped with a Janis SVT-400 variable-temperature cryostat, whereas the spectrometer used to acquire the strong-field spectra is equipped with a Janis 8TMOSS-OM-12SVT variable-temperature cryostat. The quoted isomer shifts are relative to the centroid of the spectrum of α-iron metal at room temperature. Simulations of the Mössbauer spectra were carried out using the WMOSS spectral analysis software from SEECO (www.wmoss.org; Edina, MN). Some of the simulations are based on the commonly used spin Hamiltonian (Equation 1) in which the first three terms describe the electron Zeeman effect and zero field splitting (ZFS) of the electron spin ground state, the fourth term represents the interaction between the electric field gradient and the nuclear quadrupole moment, the fifth term describes the magnetic hyperfine interactions of the electronic spin with the ^{57}Fe nucleus, and the last term represents the ^{57}Fe nuclear Zeeman interaction.

$$\begin{aligned}\mathbf{H} = \beta \mathbf{S} \bullet \mathbf{g} \bullet \mathbf{B} + D\left(\mathbf{S}_{\mathbf{z}}^2 - \frac{S(S+1)}{3}\right) + E\left(\mathbf{S}_{\mathbf{x}}^2 - \mathbf{S}_{\mathbf{y}}^2\right) \\ + \frac{\mathbf{e}\mathbf{Q}\mathbf{V}_{\mathbf{zz}}}{4}\left[\mathbf{I}_{\mathbf{z}}^2 - \frac{I(I+1)}{3} + \frac{\eta}{3}\left(\mathbf{I}_{\mathbf{x}}^2 - \mathbf{I}_{\mathbf{y}}^2\right)\right] + \mathbf{S} \bullet \mathbf{A} \bullet \mathbf{I} - g_n \beta_{\mathbf{n}} \mathbf{B} \bullet \mathbf{I}\end{aligned} \quad (1)$$

All simulations were carried out in the slow relaxation regime.

[4] a) D.F. Evans *J. Chem. Soc.* **1959**, 2003-2005. b) E.M. Schubert *J. Chem. Ed.* **1992**, *69*, 62. c) G.A. Bain, J.F Berry *J. Chem. Ed.* **2008**, *85*, 532-536.
[5] L. E. Goodrich, S. Roy, E. E. Alp, J. Zhao, M. Y. Hu, N. Lehnert, *Inorg. Chem.* **2013**, *52*, 7766-7780

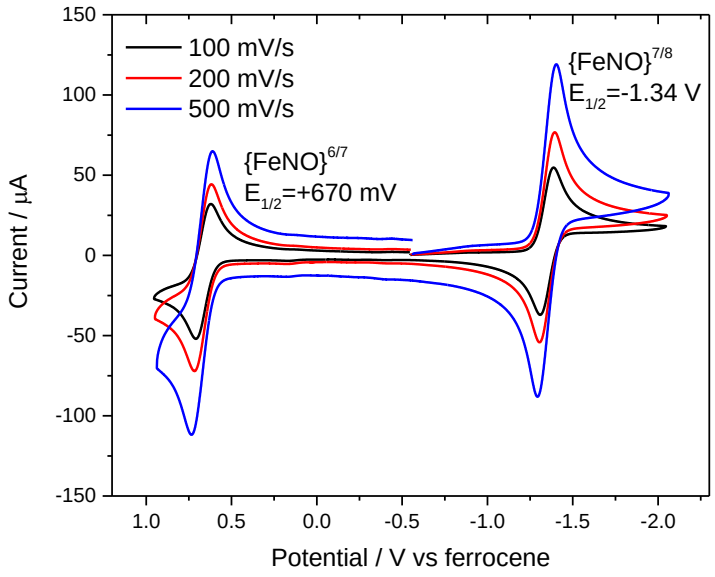

Figure S1. Cyclic voltammogram of [Fe(TMG$_3$tren)(NO)](OTf)$_2$ (**2**) at variable scan rates in CH_3CN containing 0.1 M [NBu$_4$][PF$_6$] as supporting electrolyte.

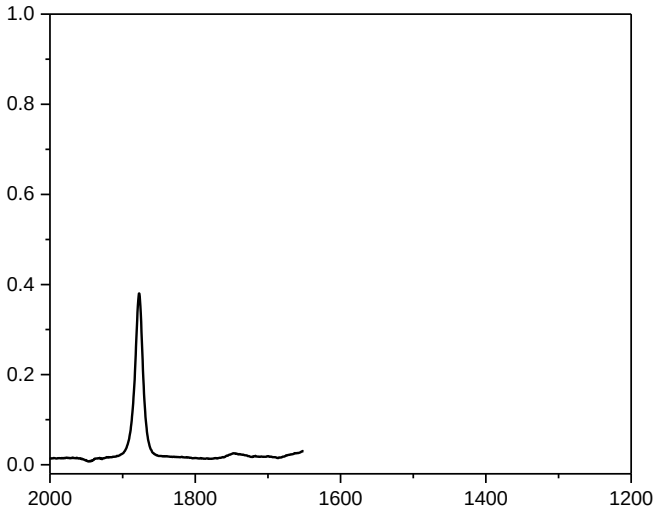

Figure S2. Solution IR showing the oxidation of [Fe(TMG$_3$tren)(NO)][(OTf)$_2$ (**2**) to the corresponding {FeNO}^{6} complex (**1**) using excess (1.3 equivalents) thianthrene tetrafluoroborate ($E_{1/2}$ = +860 mV vs ferrocene) in CD_3CN at room temperature. The oxidation is almost fully reversible upon addition of ferrocene. The peak at 1622 cm^{-1} in the re-reduced complex is the result of formation of a minor ferric impurity.

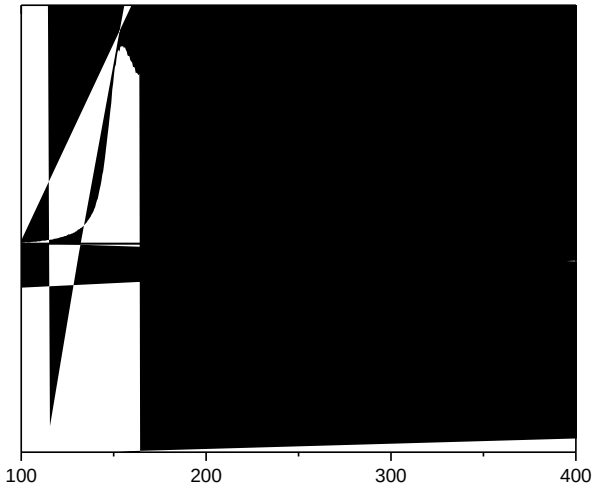

Figure S3. EPR spectra of frozen acetonitrile solutions (5 mM) showing the clean conversion of the *S* = 3/2{FeNO}^{7} complex (**2**) to the corresponding EPR-silent {FeNO}^{6} complex (**1**) upon addition of thianthrene tetrafluoroborate. Conditions: Temperature = 4.2 K; Frequency = 9.351 GHz; Microwave power = 20.5 mW; Modulation frequency = 100 kHz; Modulation amplitude = 1 G. The spectrum of **2** dissolved in acetonitrile is broader than that of **2** dissolved in CH_2Cl_2[2], suggesting that **2** exhibits greater conformational heterogeneity in acetonitrile.

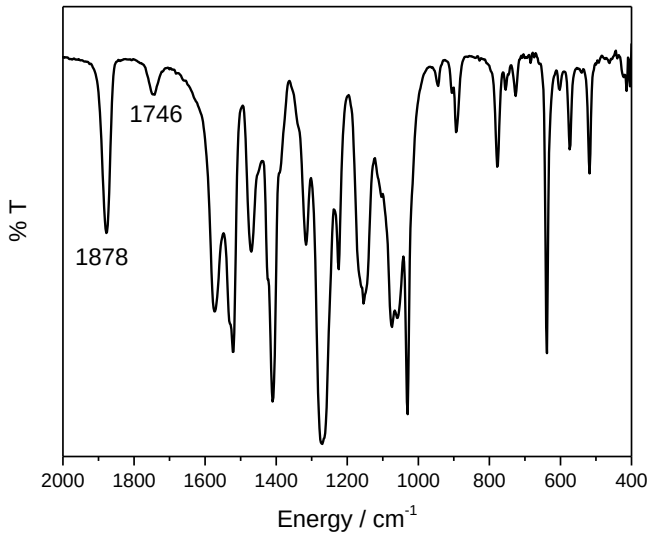

Figure S4. FT-IR spectrum (KBr pellet) of the solid {FeNO}^{6} complex **1** precipitated from an acetonitrile solution with diethyl ether. The band at 1746 cm^{-1} corresponds to a small {FeNO}^{7} impurity.

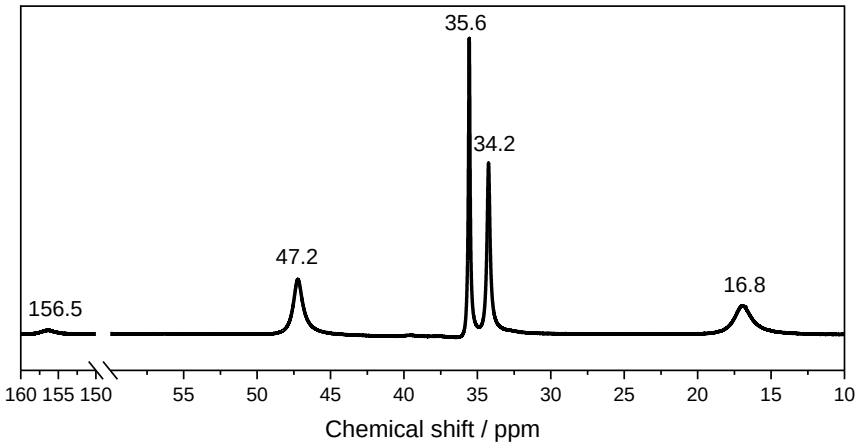

Figure S5. ^{1}H NMR spectrum (500 MHz, CD_3CN) of the $\{FeNO\}^6$ complex **1**.

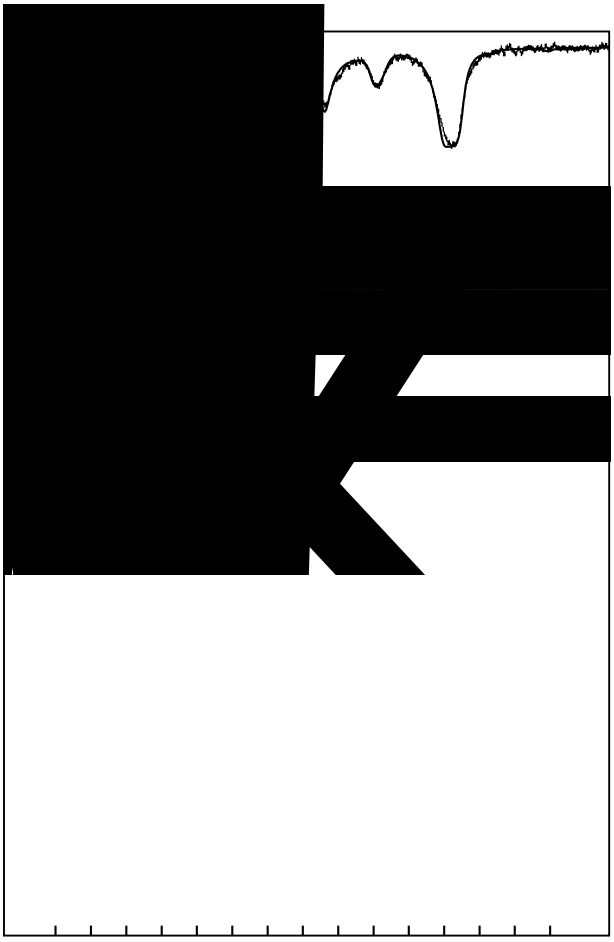

Figure S6. 4.2-K/variable-field (// = parallel, ⊥ = perpendicular magnetic field) Mössbauer spectra of a 5 mM solution of the {^{57}FeNO}^{7} complex **2** in 1:1 propionitrile:butyronitrile (black vertical bars). Spin Hamiltonian simulations carried out with respect to the total spin of the complex, S = 3/2, using the following parameters are overlaid as blue lines: D = 6.0 cm^{-1}, E/D = 0.07 (obtained independently from analysis of the X-band EPR spectrum), **g** = 2.0, δ = 0.48 mm/s, ΔE_Q = -1.42 mm/s, η = 0.08, **A** = (-21.0, -20.4, -30.0) T. These parameters are similar to those observed for other {FeNO}^{7} complexes with S = 3/2 ground state, albeit with a smaller axial zero-field splitting parameter.[6]

[6] a) S. Ye, J. C. Price, E. W. Barr, M. T. Green, J. M. Bollinger, C. Krebs, F. Neese, *J. Am. Chem. Soc.* **2010**, *132*, 4739-4751 b) C. A. Brown, M. A. Pavlosky, T. E. Westre, Y. Zhang, B. Hedman, K. O. Hodgson, E. I. Solomon, *J. Am. Chem. Soc.* **1995**, *117*, 715-732. c) C. D. Brown, M. L. Neidig, M. B. Neibergall, J. D. Lipscomb, E. I. Solomon, *J. Am. Chem. Soc.* **2007**, *129*, 7427-7438. d) D. M. Arciero, J. D. Lipscomb, B. H. Huynh, T. A. Kent, E. Münck, *J. Biol. Chem.* **1983**, *258*, 14981-14991. e) A. R. Diebold, C. D. Brown-Marshall, M. L. Neidig, J. M. Brownlee, G. R. Moran, E. I. Solomon, *J. Am. Chem. Soc.* **2011**, *133*, 18148-18160.f) A. M. Orville, V. J. Chen, A. Kriauciunas, M. R. Harpel, B. G. Fox, E. Munck, J. D. Lipscomb, *Biochemistry* **1992**, *31*, 4602-4612.

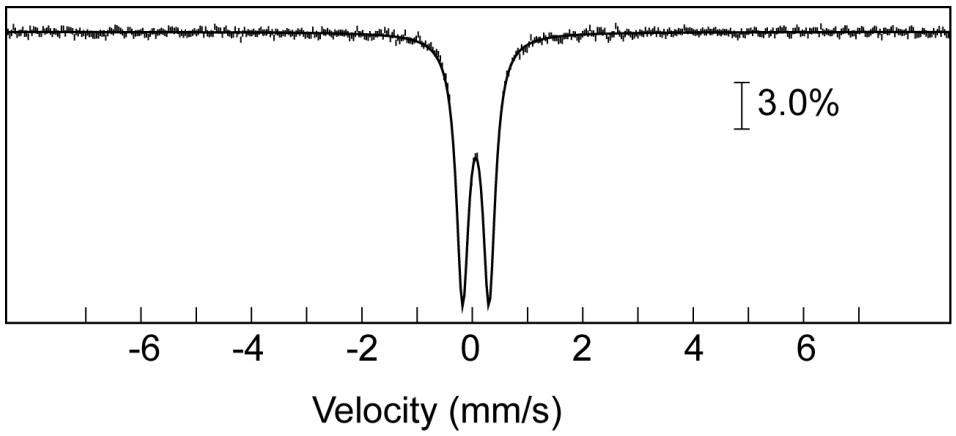

Figure S7. 4.2-K/53-mT parallel field (//) Mössbauer spectrum of a 5 mM solution of the {^{57}FeNO}^{6} complex **2** in 1:1 propionitrile:butyronitrile (black vertical bars) overlaid with a quadrupole doublet simulation using the parameters δ = 0.06 mm/s and $|\Delta E_Q|$ = 0.48 mm/s.

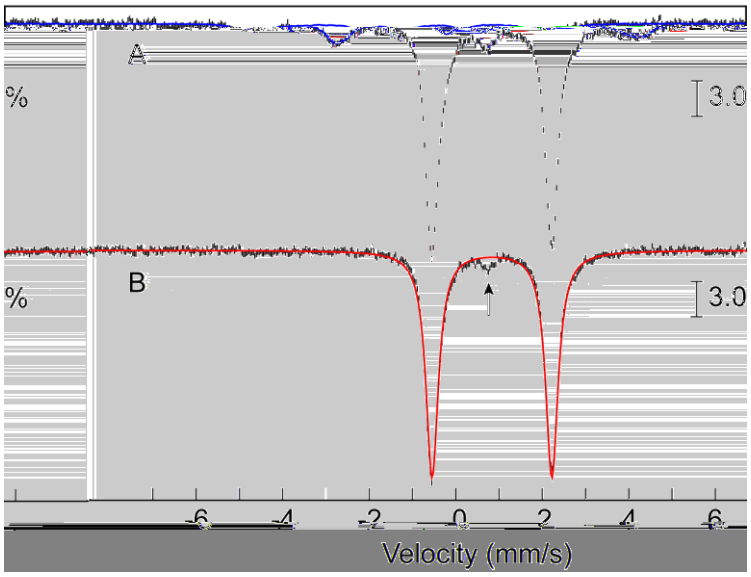

Figure S8. (**A**) 4.2-K/53-mT Mössbauer spectrum of a sample containing 5 mM solution of the {^{57}FeNO}^{8} complex **3** in 1:1 propionitrile:butyronitrile. The magnetic field was applied parallel to the γ–beam. The raw data is shown in vertical bars while the solid blue line is the experimental spectrum of {^{57}FeNO}^{7} complex **1** recorded under identical conditions and scaled to 16% of the total intensity. (**B**) Reference spectrum of the {^{57}FeNO}^{8} complex generated by removal of the contribution from the {^{57}FeNO}^{7} complex. The solid red line is the simulation of the {^{57}FeNO}^{8} complex with δ = 0.84 mm/s and $|\Delta E_Q|$ = 2.78 mm/s. The arrow points at the high-energy line of a small quadrupole doublet (~ 5%), the identity of which remains unclear.

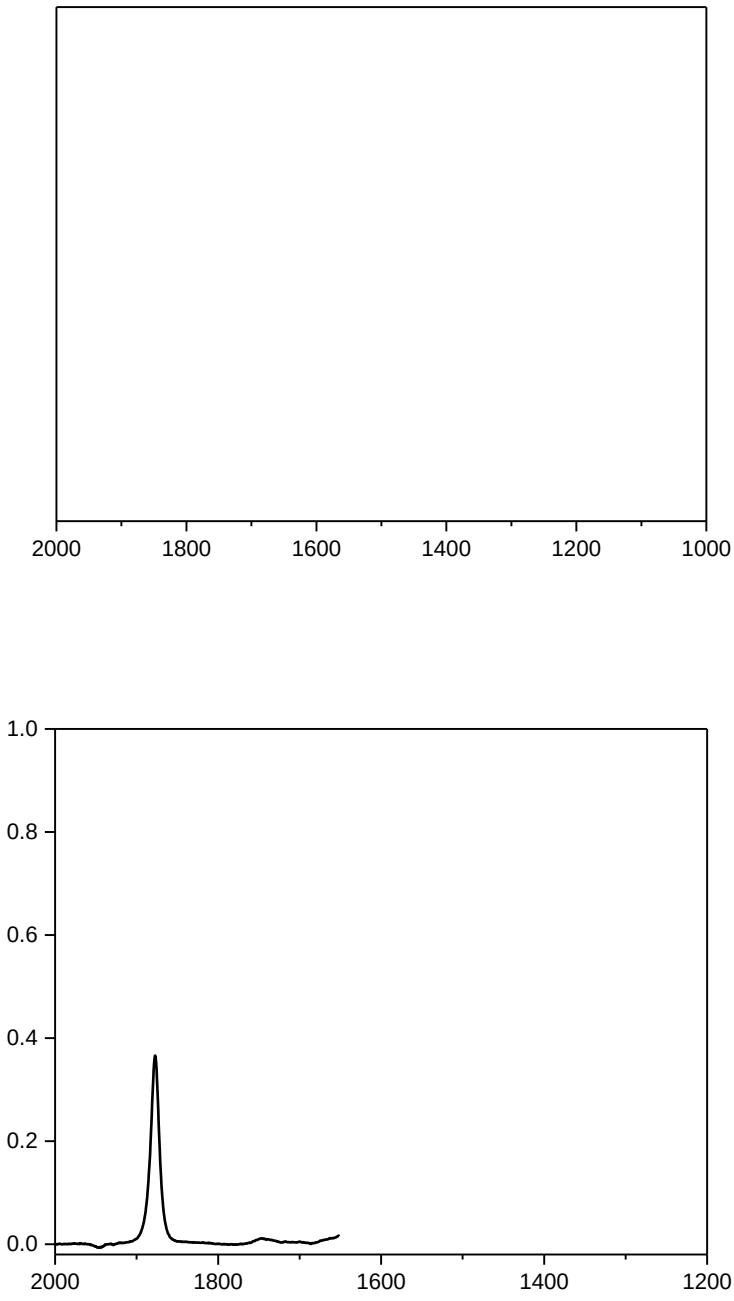

Figure S9. (Top) FT-IR spectrum (KBr pellet) of solid **1** generated in CH_3CN following the removal of solvent under vacuum. (Bottom) Solution IR of the same solid redissolved in CD_3CN (red), which is identical to the solution IR of **1** (black). These data demonstrate that NO remains bound to **1** even under vacuum.

Crystal Structure Determination[7]

At −40°C, 21.4 mg of [Fe(TMG$_3$tren)(NO)](BF$_4$)$_2$ (30.6 μmol) and 12.4 mg of thianthrene tetrafluoroborate (40.9 μmol, 1.3 equivalents) were combined in 3 mL of acetonitrile, and the resulting solution was stirred for 10 minutes. Vapor diffusion of diethyl ether into this solution at −35°C gave purple block crystals suitable for x-ray diffraction after 5 days.

A crystal of dimensions 0.26 x 0.18 x 0.16 mm was mounted on a Rigaku AFC10K Saturn 944+ CCD-based X-ray diffractometer equipped with a low temperature device and a Micromax-007HF Cu-target micro-focus rotating anode (λ = 1.54187 A) operated at 1.2 kW power (40 kV, 30 mA). The X-ray intensities were measured at 85(1) K with the detector placed at a distance of 42.00 mm from the crystal. A total of 2028 images were collected with an oscillation width of 1.0° in ω. The exposure times were 1 sec. for the low angle images, 8 sec. for high angle. Rigaku d*trek images were exported to CrysAlisPro for processing and corrected for absorption. The integration of the data yielded a total of 59818 reflections to a maximum 2θ value of 138.80° of which 7340 were independent and 7283 were greater than 2σ(I). The final cell constants (Table S1) are based on the xyz centroids of 32910 reflections above 10σ(I). Analysis of the data showed negligible decay during data collection. The structure was solved and refined with the Bruker SHELXTL (version 2014/6) software package, using the space group P2(1)/n with Z = 4 for the formula $C_{25}H_{54}B_3N_{13}OF_{12}Fe$. All non-hydrogen atoms were refined anisotropically with the hydrogen atoms placed in idealized positions. There are two acetonitrile solvate molecules disordered over four sites. Full matrix least-squares refinement based on F^2 converged at R1 = 0.0511 and wR2 = 0.1374 [based on I > 2sigma(I)], R1 = 0.0513 and wR2 = 0.1376 for all data. Additional details are presented in Table S1.

CCDC 1450725 contains the supplementary crystallographic data for this paper. These data can be obtained free of charge from the Cambridge Crystallographic Data Centre via www.ccdc.cam.ac.uk/data_request/cif.

[7] a) Sheldrick, G.M. SHELXTL, v. 2014/6; Bruker Analytical X-ray, Madison, WI, 2014. b) CrystalClear Expert 2.0 r16, Rigaku Americas and Rigaku Corporation (2014), Rigaku Americas, 9009, TX, USA 77381-5209, Rigaku Tokyo, 196-8666, Japan. c) CrysAlisPro 1.171.38.41 (Rigaku Oxford Diffraction, 2015).

Table S1. Crystal data and structure refinement for $[Fe(TMG_3tren)(NO)](BF_4)_3 \bullet 2\ CH_3CN$

Emperical formula	$C_{25}H_{54}B_3F_{12}FeN_{13}O$	
Formula weight	869.09	
Temperature	85(2) K	
Wavelength	1.54178 Å	
Crystal system	Monoclinic	
Space Group	P2(1)/n	
Unit cell dimensions	a = 10.75300(10) Å	α = 90 °
	b = 20.8943(2) Å	β = 90.3620(10) °
	c = 17.60140(10) Å	γ = 90 °
Volume	3954.54(6) $Å^3$	
Z, calculated density	4, 1.460 Mg/m^3	
Absorption coefficient	3.938 mm^{-1}	
F(0,0,0)	1808	
Crystal size	0.260 x 0.180 x 0.160 mm	
Theta range for data collection	3.283° to 69.404°	
Limiting indices	-12<=h<=13, -24<=k<=25, -21<=l<=21	
Reflections collected / unique	59818 / 7340 [R(int) = 0.0563]	
Completeness to theta = 67.679	99.9%	
Absorption correction	Semi-empirical from equivalents	
Max. and min. transmission	1.00000 and 0.50020	
Refinement method	Full-matrix least-squares on F^2	
Data / restraints/parameters	7340 / 474 / 568	
Goodness of fit on F^2	1.095	
Final R indices [I>2sigma(I)]	R1 = 0.0511, wR2 = 0.1374	
R indices (all data)	R1 = 0.0513, wR2 = 0.1376	
Extinction coefficient	0.00142(9)	
Largest diff. peak and hole	1.346 and -0.454 $e.A^{-3}$	

Computational Methods

All geometry optimizations and frequency calculations were performed with the ORCA program package[8] (version 2.9) at the TPSS[9]/def2-TZVP(-f)[10] level employing the RI approximation with the def2-TZV/J auxiliary basis set.[11] The calculated geometric parameters, N-O stretching frequencies, and Mössbauer parameters are in good agreement with experiment (Table S2). The coordinates for the DFT-optimized structures are given in Tables S4-S6. For comparison, the {FeNO}^{6} complex **1** was also optimized in the S = 0 and S = 2 spin states. These structures were 23 kcal/mol and 14 kcal/mol higher in energy, respectively, than the S = 1 structure providing further evidence that **1** has an S = 1 ground state.

Mössbauer parameters were calculated using the B3LYP[12] and TPSS functionals and the basis sets CP(PPP)[13] on Fe, TZVP[10] on N and O, and SV(P)[10] on C and H. Isomer shifts (δ) were calculated using the correlation between $\rho(0)$ (the electron density at the iron nucleus) and δ reported in the literature.[14] For both TPSS and B3LYP, the calculated Mössbauer parameters are in good agreement with experiment (Table S3). More importantly, the trends in δ (and to a lesser degree $|\Delta E_Q|$) are well-reproduced (Figures S10 and S11) for both the {FeNO}$^{6\text{-}8}$ and other TMG_3tren complexes, indicating that DFT is able to properly replicate changes in electronic structure in TMG_3tren compounds.

In order to examine bonding, single-point calculations were performed at the B3LYP/def2-TZVP(-f) level employing the RIJCOSX[15] approximation with the def2-TZV/J auxiliary basis set. To facilitate comparison between the {FeNO}^{6}, {FeNO}^{7}, and {FeNO}^{8} complexes, the canonical orbitals for the broken symmetry solutions were transformed into unrestricted corresponding orbitals (UCOs).[16] Note that because of the underlying transformation, the orbital energies for the UCOs are not well-defined. The orbitals were plotted using the orca_plot tool and visualized using Molekel version 5.4[17] (electron density isosurface value = 0.05).

[8] F. Neese, *Wiley Interdiscip. Rev.: Comput. Mol. Sci.* **2012**, *2*, 73-78.
[9] a) J. Tao, J. P. Perdew, V. N. Staroverov, G. E. Scuseria, *Phys. Rev. Lett.* **2003**, *91*, 146401. b) J. P. Perdew, J. Tao, V. N. Staroverov, G. E. Scuseria, *J. Chem. Phys.* **2004**, *120*, 6898-6911.
[10] a) A. Schäfer, H. Horn, R. Ahlrichs, *J. Chem. Phys.* **1992**, *97*, 2571-2577. b) F. Weigend, R. Ahlrichs, *PCCP* **2005**, *7*, 3297-3305.
[11] a) K. Eichkorn, O. Treutler, H. Öhm, M. Häser, R. Ahlrichs, *Chem. Phys. Lett.* **1995**, *240*, 283-290. b) K. Eichkorn, F. Weigend, O. Treutler, R. Ahlrichs, *Theor. Chem. Acc.* **1997**, *97*, 119-124.
[12] a) A. D. Becke, *J. Chem. Phys.* **1993**, *98*, 5648-5652. b) C. Lee, W. Yang, R. G. Parr, *Phys. Rev. B* **1988**, *37*, 785-789.
[13] F. Neese, *Inorg. Chim. Acta* **2002**, *337*, 181-192.
[14] M. Römelt, S. Ye, F. Neese, *Inorg. Chem.* **2009**, *48*, 784-785.
[15] F. Neese, F. Wennmohs, A. Hansen, U. Becker, *Chem. Phys.* **2009**, *356*, 98-109.
[16] F. Neese, *J. Phys. Chem. Solids* **2004**, *65*, 781-785.
[17] U. Varetto, Molekel 5.4

Table S2. Comparison of DFT-calculated geometric parameters and N-O stretching frequencies to experimental values.

	{FeNO}^{6} Expt.	{FeNO}^{6} DFT	{FeNO}^{7} Expt.	{FeNO}^{7} DFT	{FeNO}^{8} Expt.	{FeNO}^{8} DFT
Fe-N(O) (Å)	1.680	1.666	1.748	1.721	--	1.694
N-O (Å)	1.142	1.151	1.154	1.177	--	1.202
Fe-N-O (°)	180	180	168	154	--	159
Fe-N$_{amine}$ (Å)	2.020	2.042	2.251	2.222	--	2.112
Avg. Fe-N$_{guan}$ (Å)	1.966	2.008	2.037	2.071	--	2.313
ν(NO) (cm^{-1})	1878[a,b]	1874	1730-1740[a,c] 1750[b]	1714	1618[b]	1628

[a] Solid state (KBr pellet) [b] In CD_3CN solution [c] The NO stretch of the {FeNO}^{7} complex **1** in the solid state varies depending on the conditions of isolation. However, regardless of the solid-state NO stretch, all compounds exhibit ν(NO) = 1750 cm^{-1} upon redissolving in CD_3CN solution.

Table S3. Comparison of DFT-calculated Mössbauer parameters to experimental values.

	δ (mm/s)			$\|\Delta E_Q\|$ (mm/s)		
	Expt.	**B3LYP**	**TPSS**	**Expt.**	**B3LYP**	**TPSS**
{FeNO}^{8} (3)	0.84	0.72	0.81	2.78	2.13	1.62
{FeNO}^{7} (2)	0.48	0.38	0.52	1.42	1.69	1.33
{FeNO}^{6} (1)	0.06	0.07	0.19	0.48	0.40	0.49
Fe(IV)=O[18]	0.09	0.07	0.19	0.29	0.55	0.46
Fe(IV)-CN[19]	-0.19	-0.21	-0.10	4.45	5.25	4.76

[18] J. England, M. Martinho, E. R. Farquhar, J. R. Frisch, E. L. Bominaar, E. Münck, L. Que Jr., *Angew. Chem.* **2009**, *121*, 3676-3680; *Angew. Chem. Int. Ed.* **2009**, *48*, 3622-3626.
[19] J. England, E. R. Farquhar, Y. Guo, M. A. Cranswick, K. Ray, E. Münck, L. Que Jr., *Inorg. Chem.* **2011**, *50*, 2885-2896.

Table S4. Coordinates for the TPSS/def2-TZVP(-f)-optimized structure of the {FeNO}^{6} complex **1**

	X	Y	Z
Fe	0.00593	-0.01618	0.4616
N	0.00751	0.0045	-1.20466
N	0.00433	-0.0409	2.50298
N	1.31575	-1.52234	0.68233
N	-1.95142	-0.4025	0.69334
N	0.65352	1.86694	0.72275
N	3.2011	-2.72979	-0.11445
N	1.19989	-2.78539	-1.31008
N	-3.94804	-1.41725	-0.10065
N	-3.00623	0.36223	-1.27697
N	0.76395	4.11792	-0.03083
N	1.82716	2.436	-1.24657
C	0.59671	-1.34646	2.96762
H	-0.17024	-2.11691	2.87149
H	0.87558	-1.25698	4.02379
C	1.78123	-1.66965	2.08497
H	2.62255	-1.00481	2.30876
H	2.11651	-2.69443	2.27242
C	1.91361	-2.33118	-0.24669
C	4.26321	-1.88374	0.45665
H	3.91829	-0.85495	0.53851
H	5.12433	-1.91767	-0.21747
H	4.57832	-2.25524	1.43693
C	3.65501	-4.08437	-0.50782
H	2.79583	-4.73088	-0.67806
H	4.24623	-4.48871	0.31867
H	4.28356	-4.04726	-1.40225
C	1.827	-3.09416	-2.60996
H	2.81063	-2.62962	-2.66639
H	1.18924	-2.68241	-3.39836
H	1.91761	-4.17288	-2.77005
C	-0.19844	-3.21926	-1.18592
H	-0.54751	-3.01176	-0.17643
H	-0.26007	-4.29519	-1.3842
H	-0.82741	-2.70087	-1.91676
C	-1.41821	0.08988	2.98314
H	-1.70297	1.1408	2.90863
H	-1.47049	-0.2156	4.03445
C	-2.29832	-0.75819	2.09294
H	-2.1407	-1.82315	2.29533

H	-3.35169	-0.54032	2.29448
C	-2.95981	-0.49999	-0.2277
C	-3.74193	-2.76891	0.44759
H	-2.67792	-2.98662	0.51564
H	-4.2091	-3.48685	-0.23317
H	-4.21165	-2.87099	1.43108
C	-5.35176	-1.1262	-0.47565
H	-5.48277	-0.05644	-0.62928
H	-5.98946	-1.44736	0.35278
H	-5.64341	-1.67603	-1.37515
C	-3.60216	-0.00498	-2.57641
H	-3.69328	-1.08799	-2.6493
H	-2.93533	0.35369	-3.36664
H	-4.58303	0.45906	-2.71795
C	-2.67937	1.78758	-1.13364
C	0.83304	1.11647	2.99779
H	1.8848	0.83908	2.90951
H	0.60333	1.29502	4.0545
C	0.53116	2.31898	2.13224
H	-0.46813	2.71102	2.35064
H	1.24834	3.11846	2.34249
C	1.06485	2.80642	-0.18444
C	-0.50659	4.60341	0.53482
H	-1.22567	3.78873	0.59284
H	-0.90028	5.37869	-0.12932
H	-0.35412	5.04346	1.52548
C	1.71411	5.19607	-0.39218
H	2.70576	4.779	-0.55894
H	1.75858	5.894	0.44866
H	1.37783	5.73905	-1.28016
C	1.7955	3.15864	-2.53314
H	0.9014	3.7784	-2.58795
H	1.76782	2.41592	-3.33653
H	2.68547	3.78027	-2.67072
C	2.90075	1.4396	-1.12967
H	2.88386	1.01351	-0.12862
H	3.8655	1.92797	-1.30701
H	2.77499	0.65048	-1.87794
O	0.00867	0.01919	-2.35598
H	-1.92403	2.08379	-1.86859
H	-2.31318	1.96956	-0.12529
H	-3.58169	2.38317	-1.31204

Table S5. Coordinates for the TPSS/def2-TZVP(-f)-optimized structure of the {FeNO}^{7} complex **2**

	X	Y	Z
Fe	-0.02639	-0.01152	0.29165
N	-0.02659	0.03476	-1.42904
N	-0.03116	-0.05652	2.51271
N	1.25883	-1.63939	0.63271
N	-2.04717	-0.3005	0.63405
N	0.75221	1.84347	0.64336
N	3.04822	-3.03278	-0.10575
N	1.05266	-2.95527	-1.29866
N	-4.13038	-1.15111	-0.14433
N	-3.13108	0.65805	-1.21433
N	1.12975	4.08845	-0.05091
N	2.16564	2.33513	-1.17179
C	0.59091	-1.33933	2.94877
H	-0.17133	-2.11985	2.88336
H	0.92244	-1.2721	3.99376
C	1.7501	-1.68677	2.02424
H	2.57495	-0.98029	2.18615
H	2.12825	-2.68363	2.27659
C	1.78821	-2.51707	-0.23528
C	4.17985	-2.25699	0.41397
H	3.91759	-1.20151	0.45283
H	5.02984	-2.38299	-0.26492
H	4.48054	-2.59837	1.41079
C	3.36857	-4.42781	-0.45358
H	2.44926	-4.98649	-0.62456
H	3.90349	-4.87825	0.38869
H	4.00661	-4.48621	-1.34198
C	1.65643	-3.28913	-2.59514
H	2.68901	-2.9428	-2.6216
H	1.09077	-2.78014	-3.38296
H	1.62818	-4.36675	-2.79121
C	-0.39051	-3.17566	-1.21062
H	-0.71557	-2.96536	-0.1929
H	-0.61168	-4.21992	-1.46301
H	-0.93073	-2.5262	-1.90731
C	-1.44994	0.03451	2.96185
H	-1.74715	1.08584	2.93397
H	-1.55242	-0.32277	3.99537
C	-2.32804	-0.76504	2.01071
H	-2.12068	-1.83661	2.12556

H	-3.38164	-0.61064	2.26766
C	-3.08363	-0.27948	-0.22539
C	-3.97337	-2.54478	0.28801
H	-2.91846	-2.81235	0.29033
H	-4.49992	-3.19025	-0.42251
H	-4.39838	-2.7082	1.28455
C	-5.51632	-0.75339	-0.44843
H	-5.57774	0.32982	-0.54393
H	-6.15469	-1.07129	0.38198
H	-5.87842	-1.22681	-1.36711
C	-3.73285	0.3963	-2.52899
H	-3.91095	-0.6721	-2.64636
H	-3.03077	0.72652	-3.30157
H	-4.67434	0.94091	-2.66019
C	-2.65964	2.02846	-1.00678
C	0.7594	1.12146	2.96758
H	1.81867	0.85599	2.92507
H	0.51236	1.3787	4.00648
C	0.49184	2.29165	2.03273
H	-0.5425	2.63737	2.15451
H	1.14599	3.12894	2.29742
C	1.32538	2.74373	-0.18289
C	-0.14986	4.6688	0.37279
H	-0.92567	3.90632	0.34745
H	-0.41786	5.46896	-0.32496
H	-0.08382	5.09553	1.37976
C	2.20187	5.07103	-0.28928
H	3.15918	4.55924	-0.37863
H	2.24203	5.74873	0.56943
H	2.01357	5.66286	-1.19119
C	2.29007	3.04606	-2.45296
H	1.48776	3.77614	-2.54942
H	2.20196	2.31472	-3.26248
H	3.25857	3.54977	-2.54105
C	3.02502	1.15994	-1.02999
H	2.9265	0.77102	-0.01803
H	4.06431	1.45401	-1.2175
H	2.74939	0.38178	-1.74971
O	-0.0499	0.58054	-2.47106
H	-1.83952	2.26875	-1.6907
H	-2.32328	2.13108	0.02385
H	-3.48538	2.7247	-1.19648

Table S6. Coordinates for the TPSS/def2-TZVP(-f)-optimized structure of the {FeNO}^{8} complex **3**

	X	Y	Z
Fe	-0.01251	-0.08646	0.13172
N	-0.08741	0.0609	-1.55431
O	-0.41508	0.48916	-2.62863
N	0.0429	-0.12186	2.49035
N	1.95052	-0.95566	0.62122
N	-1.80242	-1.15491	0.64859
N	-0.16072	1.98342	0.61446
N	4.18369	-1.39944	-0.10138
N	2.3719	-2.31572	-1.23628
N	-3.34887	-2.82148	-0.08198
N	-3.34099	-0.7088	-1.06115
N	-0.73351	4.22776	0.04459
N	0.92913	3.11086	-1.13905
C	1.2205	-0.91003	2.92639
H	0.94971	-1.96911	2.87857
H	1.49081	-0.67543	3.9682
C	2.39716	-0.6605	1.98683
H	2.72766	0.38337	2.08682
H	3.24124	-1.29536	2.2871
C	2.81148	-1.52003	-0.2074
C	4.8266	-0.15893	0.32705
H	4.09287	0.64488	0.34789
H	5.61231	0.104	-0.3918
H	5.28623	-0.25548	1.31893
C	5.09736	-2.49795	-0.42514
H	4.5254	-3.41118	-0.58772
H	5.78371	-2.65315	0.41585
H	5.69447	-2.28139	-1.32045
C	2.96568	-2.25821	-2.57376
H	3.79805	-1.55494	-2.57709
H	2.21232	-1.91422	-3.29314
H	3.3258	-3.24474	-2.88975
C	1.1165	-3.05353	-1.14319
H	0.83034	-3.1224	-0.09334
H	1.26974	-4.06087	-1.55037
H	0.31273	-2.56003	-1.70066
C	-1.22316	-0.7404	2.95821
H	-1.98549	0.04153	3.00976
H	-1.10383	-1.16483	3.96686

C	-1.67533	-1.80209	1.96313
H	-0.93788	-2.61824	1.94447
H	-2.6284	-2.23527	2.29211
C	-2.78622	-1.55978	-0.14015
C	-2.54505	-4.01599	0.16271
H	-1.4886	-3.76576	0.07521
H	-2.789	-4.77373	-0.5921
H	-2.73378	-4.44646	1.15487
C	-4.78257	-3.05185	-0.27241
H	-5.30138	-2.09435	-0.31492
H	-5.17198	-3.62922	0.57497
H	-4.98596	-3.61343	-1.19347
C	-3.72477	-1.15143	-2.40408
H	-3.52946	-2.21851	-2.50823
H	-3.13034	-0.61005	-3.14907
H	-4.78791	-0.95959	-2.59395
C	-3.33271	0.73574	-0.85489
C	0.13939	1.29328	2.92174
H	1.19001	1.59327	2.87676
H	-0.2028	1.41162	3.96206
C	-0.66708	2.18056	1.979
H	-1.7314	1.91437	2.04714
H	-0.56907	3.2255	2.29852
C	-0.00473	3.064	-0.1344
C	-2.15296	4.21349	0.38633
H	-2.53413	3.19653	0.31111
H	-2.70211	4.84771	-0.32116
H	-2.33612	4.59312	1.40027
C	-0.13571	5.55612	-0.10197
H	0.94135	5.4577	-0.23662
H	-0.32762	6.14268	0.80514
H	-0.55717	6.09962	-0.9577
C	0.66821	3.77117	-2.42007
H	-0.33522	4.19561	-2.4166
H	0.73343	3.03337	-3.22803
H	1.39722	4.56892	-2.609
C	2.14992	2.31793	-1.08285
H	2.24506	1.89679	-0.08282
H	3.00818	2.96631	-1.30391
H	2.12917	1.49773	-1.80915
H	-2.56299	1.22598	-1.45987
H	-3.14257	0.93385	0.1996
H	-4.31467	1.13615	-1.13646